Summer Extreme Cyclone Impacts on Arctic Sea Ice

JENNIFER V. LUKOVICH,[a] JULIENNE C. STROEVE,[a,b,c] ALEX CRAWFORD,[a] LAWRENCE HAMILTON,[d] MICHEL TSAMADOS,[c] HARRY HEORTON,[c] AND FRANÇOIS MASSONNET[e]

[a] *Centre for Earth Observation Science, University of Manitoba, Winnipeg, Manitoba, Canada*
[b] *National Snow and Ice Data Center, University of Colorado, Boulder, Colorado*
[c] *Centre for Polar Observation and Modelling, Earth Sciences, University College London, London, United Kingdom*
[d] *Department of Sociology, University of New Hampshire, Durham, New Hampshire*
[e] *Centre de Recherches sur la Terre et le Climat Georges Lemaître, Earth and Life Institute, Université Catholique de Louvain, Louvain-la-Neuve, Belgium*

(Manuscript received 10 December 2019, in final form 22 February 2021)

ABSTRACT: In this study the impact of extreme cyclones on Arctic sea ice in summer is investigated. Examined in particular are relative thermodynamic and dynamic contributions to sea ice volume budgets in the vicinity of Arctic summer cyclones in 2012 and 2016. Results from this investigation illustrate that sea ice loss in the vicinity of the cyclone trajectories during each year was associated with different dominant processes: thermodynamic processes (melting) in the Pacific sector of the Arctic in 2012, and both thermodynamic and dynamic processes in the Pacific sector of the Arctic in 2016. Comparison of both years further suggests that the Arctic minimum sea ice extent is influenced by not only the strength of the cyclone, but also by the timing and location relative to the sea ice edge. Located near the sea ice edge in early August in 2012, and over the central Arctic later in August in 2016, extreme cyclones contributed to comparable sea ice area (SIA) loss, yet enhanced sea ice volume loss in 2012 relative to 2016. Central to a characterization of extreme cyclone impacts on Arctic sea ice from the perspective of thermodynamic and dynamic processes, we present an index describing relative thermodynamic and dynamic contributions to sea ice volume changes. This index helps to quantify and improve our understanding of initial sea ice state and dynamical responses to cyclones in a rapidly warming Arctic, with implications for seasonal ice forecasting, marine navigation, coastal community infrastructure, and designation of protected and ecologically sensitive marine zones.

KEYWORDS: Arctic; Sea ice; Dynamics; Extreme events; Storm tracks; Thermodynamics

1. Introduction

Over the last four decades, the Arctic Ocean has lost over 40% of its summer sea ice cover (e.g., Stroeve and Notz 2018). This loss, together with an increasing desire to utilize the Arctic's abundant natural resources and potential shipping routes, provides for increased marine access throughout the Arctic Ocean. This access has increased the need for reliable sea ice forecasts, especially at 1–3-month lead times. In response, the Study of Environmental Arctic Change (SEARCH) began soliciting sea ice outlooks (SIOs) in 2008 for the September sea ice extent (SIE). This informal effort was transformed into the funded Sea Ice Prediction Network (SIPN), which solicits SIOs for September SIE in June, July, and August each summer. In the early years, forecasts were primarily based on statistical forecast models or heuristic approaches, but these have steadily evolved to using more advanced dynamical coupled ice–ocean or fully coupled ice–ocean–atmospheric models. Evaluation of these forecasts has revealed that regardless of method, forecasts struggle when the observed SIE minima depart strongly from the linear trend (e.g., Stroeve et al. 2014; Hamilton and Stroeve 2016).

Several studies have shown that sea ice loss is linearly related to global mean warming (e.g., Notz and Stroeve 2018; Olonscheck et al. 2019; Notz and SIMIP Community 2020). Thus, one may expect the observed September SIE to fall somewhere close to this linear trend line as temperatures increase each year. However, departures from this line strongly reflect changes in atmospheric circulation (Figs. 1a–c). For example, in 2012 the September SIE fell more than three standard deviations below the climatological (1981–2010) average, hitting the lowest extent observed yet during the satellite data record. This record low was in part attributed to an unusually strong cyclone that entered the Arctic Ocean in early August (Simmonds and Rudeva 2012; Parkinson and Comiso 2013; Zhang et al. 2013; Guemas et al. 2013). Median SIO predictions in June, July, and August 2012 (submitted before the cyclone) were far above the observed September extent (Figs. 1d–f).

Prediction difficulties resulting from the 2012 cyclone echoed into the following year; in 2013, most SIO contributors expected a similarly low extent. But that summer experienced generally cooler weather and no similar extreme cyclone event, resulting instead in an unexpectedly high September extent relative to forecasts, and also falling above the long-term linear trend line. Thus, this single extreme event in 2012 likely

Denotes content that is immediately available upon publication as open access.

Supplemental information related to this paper is available at the Journals Online website: https://doi.org/10.1175/JCLI-D-19-0925.s1.

Corresponding author: J. V. Lukovich, jennifer.lukovich@umanitoba.ca

DOI: 10.1175/JCLI-D-19-0925.1

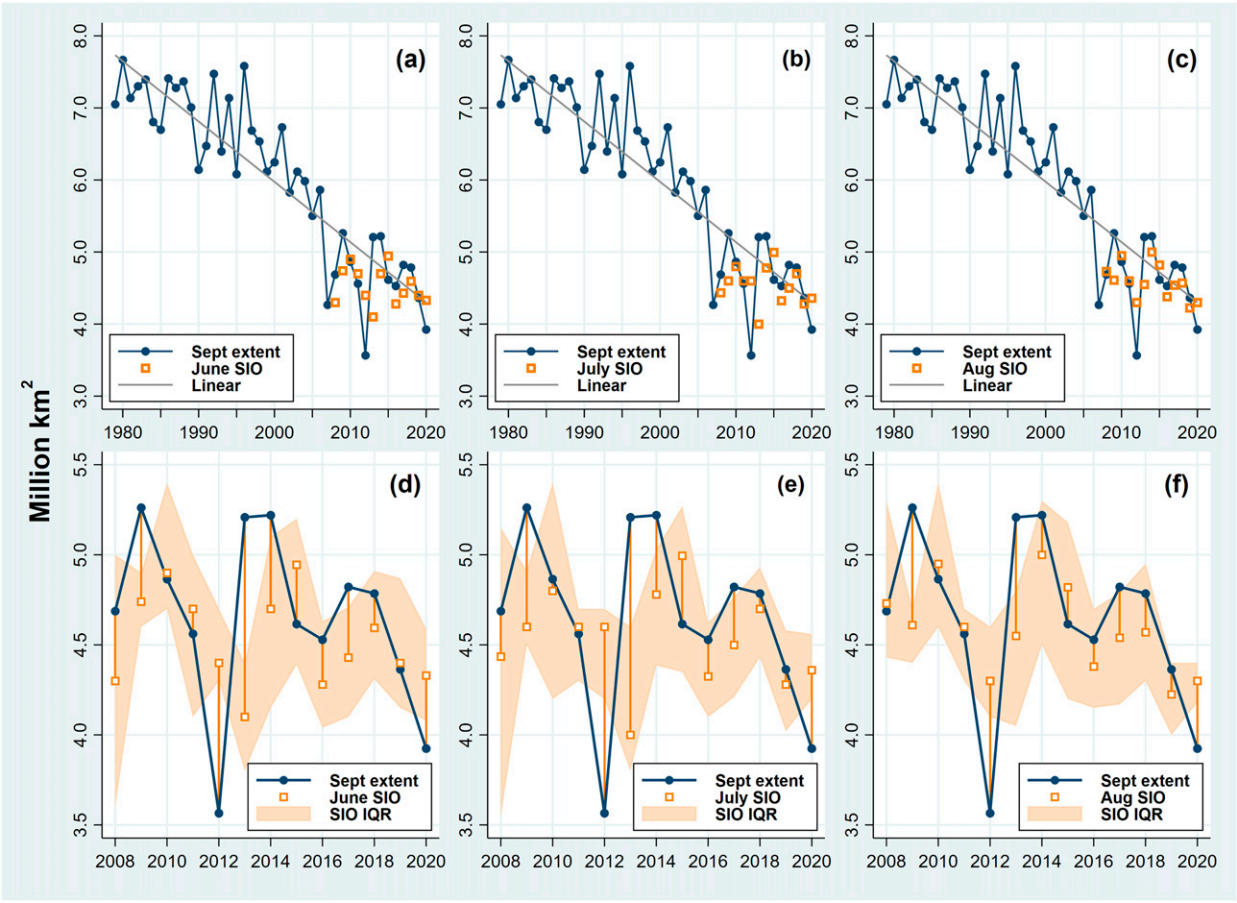

FIG. 1. Observed September Arctic sea ice extent, compared with more than 1000 sea ice outlook (SIO) predictions submitted in June, July, or August of 2008–20, show unanticipated departures from the linear trend, SIO median, and SIO interquartile range (IQR; methods described in Hamilton and Stroeve 2016).

contributed to the two least successful years of sea ice prediction: the observed September SIE in 2012 and 2013 fell well outside the interquartile range of June, July, or August predictions.

Recent analysis led by SIPN highlights the need to understand the drivers of abrupt year-to-year variations in SIE, in which synoptic drivers and extreme events play a role (see Fig. S1 in the online supplemental material). Here it was shown that regardless of method, forecasts are influenced by last year's SIE observations, contributing to poor forecast skill (Figs. S1a–d). As a specific example, September SIE predictions determined from values extrapolated based on the difference between 2012 (2016) and 2011 (2015) SIE on 1 June, 1 July, and 1 August, following Meier (Sea Ice Outlook, 2016–19; https://www.arcus.org/sipn/sea-ice-outlook; Figs. S1e,f), are shown to overestimate the September extent in 2012. By contrast, predictions based on the 2015 rate underestimate and approximate the 2016 SIE.

Given the importance of summer weather conditions on the evolution of the ice cover, several studies have looked to the role of cyclonic versus anticyclonic conditions (Kwok 2006; Wernli and Papritz 2018; Wang et al. 2020). Cyclone frequency peaks during summer (Simmonds et al. 2008; Serreze and Barrett 2008; Rudeva and Simmonds 2015; Crawford and Serreze 2016) as storms migrate from the Eurasian continent (especially along the Arctic coastline) to the North Atlantic storm track and develop locally (Serreze and Barrett 2008; Sorteberg and Walsh 2008; Simmonds and Keay 2009; Crawford and Serreze 2016). The impact of summer cyclone activity on sea ice loss was first noted in a study by Serreze et al. (2003), who showed that persistence of anomalously low SLP conditions in June, July, and August 2002 preceded the September minimum SIE, which reached a new record low that year. While the spatial patterns of the center of the low pressure systems across the Arctic Ocean varied each month, the cyclones induced sea ice divergence, which combined with higher than average air temperatures, enhanced summer ice melt (Serreze et al. 2003). On the other hand, a study by Screen et al. (2011) suggested that high cyclone activity in May, June, and July leads to higher than average September SIEs, according to the argument that increased cyclone activity is associated with stronger sea ice cyclonic circulation, divergence, and thus expansion in the ice cover. During anticyclonic conditions, clear-sky conditions enhance incoming solar radiation and thus summertime sea ice melt (Knudsen et al. 2015; Kay et al. 2008).

Since the study by Serreze et al. (2003), both the lowest and third lowest record minima in SIE, in 2012 and 2016 respectively, have similarly been characterized by persistent anomalously low sea level pressure regimes, but were additionally influenced by extreme cyclones, referred to in the literature and media as great Arctic cyclone events (Simmonds and Rudeva 2012). Specifically, the "Great Arctic Cyclone" of 6 August 2012 was found to have had a significant impact on a weakened and thinner ice cover (Simmonds and Rudeva 2012). Similarly, the extreme Arctic cyclone on 16 August 2016 occurred in a year with the third lowest record minimum in SIE.

Previous studies have explored the impact of cyclones on sea ice concentration (SIC) (Kriegsmann and Brümmer 2014; Lynch et al. 2016; Jakobson et al. 2019; Schreiber and Serreze 2020; Finocchio et al. 2020). In a statistical analysis of cyclone impacts, Kriegsmann and Brümmer (2014) documented a decrease in SIC near the cyclone center that amplifies with cyclone intensity due to divergence and deformation. An assessment of cumulative storm impact further demonstrated that in summer, sea ice loss extends beyond the cyclone radius and that overall ice loss is accelerated due to enhanced melt. Also noted was an apparent contradiction between this and previous findings showing correspondence between enhanced SIE and spring and summer cyclone activity (Screen et al. 2011), attributed in part to local and regional characterizations consistent with Lynch et al. (2016), who highlighted regional asymmetry in sea ice response to atmospheric circulation regimes. More recently, Jakobson et al. (2019) showed that winds exceeding 5 m s^{-1} (characteristic of intense storms) resulted in enhanced SIC reduction in summer, while Schreiber and Serreze (2020) demonstrated a SIC decrease (increase) in the central Arctic (coastal regions) in response to storms in summer. Finocchio et al. (2020) also indicated that cyclones' suppression in SIE decline due to cloud cover in May and June ends in July and August, and that storm-related factors other than winds and atmospheric energy fluxes contribute to late summer SIE variability. Neglected in each of these studies however is the impact on thickness and thus volume changes, as well as the role of storms in complicating sea ice predictability over time scales ranging from weeks to months.

SIE forecasts are influenced by several uncertainty sources, and observed SIE by multiple factors including persistent storms characterized by seasonal time scales and extreme cyclones characterized by weekly time scales. Extreme storms, defined here as those for which the sea level pressure (SLP) drops below 985 hPa poleward of 60°N (Rinke et al. 2017), create an additional complication in providing accurate forecasts. The purpose of this study is to use extreme cyclones as examples, while developing tools that can help characterize storm impacts on sea ice conditions, and which could further be used to improve our understanding of ice conditions preceding the September SIE. Here we explore extreme storm impacts on summer sea ice volume, and in particular address three research questions:

1) How do the spatial distribution and timing of extreme August storms in 2012 and 2016 differ?
2) What was the impact of these two August storms on the following September sea ice cover from the perspective of thermodynamic and dynamic contributions to the sea ice volume budgets?
3) Although both 2012 and 2016 are characterized by great Arctic cyclone events, what differences in cyclone behavior contribute to observed differences in SIE and enhanced loss in 2012?

Implicit in these research questions is a search for improved understanding of summer storm impacts on sea ice as one factor that can improve sea ice forecast skill on time scales ranging from weeks (as investigated here) to months. Through characterization of the sea ice volume budgets in the vicinity of cyclone tracks in August 2012 and 2016, we suggest that storm timing and location in summer may be more relevant indicators of storm impacts than frequency and intensity, and that cyclone activity, particularly within a vulnerable sea ice regime of reduced thickness, contributes to enhanced sea ice loss. Section 2 presents the data and methods used to characterize relative thermodynamic and dynamic contributions to changes in Arctic sea ice volume, followed by a description of results in section 3, discussion in section 4, and conclusions in section 5 summarizing findings and examining the implications for (emergency) planning and preparedness in the Arctic and beyond in the context of a changing climate.

2. Data and methods

Cyclone tracks are derived from 6-h ERA-Interim SLP fields using the Lagrangian detection and tracking algorithm described in full by Crawford and Serreze (2016). This algorithm detects cyclone centers as minima in SLP for which the average SLP difference between the minimum and all grid cells that intersect a radius of 1000 km is at least 7.5 hPa. Cyclone area is calculated as the last closed isobar, meaning that the isobar contains no other minima retained as cyclone centers and no SLP maxima. SLP fields are reprojected to an equal-area grid with a 100-km resolution prior to detection, and elevations greater than 1500 m are masked out. Cyclone tracking from one observation time (t_n) to the next (t_{n+1}) has three steps. First, candidate cyclones in t_n are limited to a maximum propagation speed of 150 km h^{-1}. Next, past propagation of the cyclone track at t_n is used to predict a most likely continuation in t_{n+1}. The closest candidate cyclone center existing in t_{n+1} to that predicted location is chosen as the continuation of a track. Third, special cyclone events such as cyclogenesis (origination) and cyclolysis (termination), and merging or splitting of storms are recorded. Several cyclone characteristics are recorded for each observation, including central pressure, cyclone intensity (defined as the Laplacian in the SLP), and radius (defined as the radius of a circle with an area equivalent to that of the cyclone). Cyclone trajectories are examined from 1 July to 30 August in 2012 and 2016. The most intense storms in both 2012 and 2016 experienced a merge event, which was verified by manual inspection of the tracks.

The various decisions made while automating the detection and tracking of cyclones such as the choice of input variable (Vessey et al. 2020) or parameters like elevation masking or maximum-allowed propagation speed (Rudeva et al. 2014) lead to significant variability in the resulting statistics. As seen in the supplemental material of Crawford and Serreze (2016),

this algorithm yields cyclone center frequency within the range of algorithms compared by Neu et al. (2013). Differences in cyclone detection and tracking scheme and the reanalysis used tend to be less pronounced for larger and more intense storms (Pinto et al. 2005; Neu et al. 2013; Vessey et al. 2020), which reduces issues of sensitivity in this study. Simmonds and Rudeva (2014) further demonstrated consensus among storm tracking algorithms in identifying extreme storm characteristics, including the evolution in and location of central pressure systems at greatest intensity, indicating that results from individual schemes are typical of an ensemble of storm tracking methods. The algorithm used in the present study is an extension of Serreze (1995), referred to as M09 in Simmonds and Rudeva (2014).

NSIDC daily Polar Pathfinder sea ice motion (version 4) vectors $\mathbf{u}$ and PIOMAS daily effective thickness H_{eff} data are used to compute the ice volume budget according to the continuity equation (Bitz et al. 2005)

$$\frac{\partial V}{\partial t} = D + T$$

for the volume $V = H_{\text{eff}} = CH$ (the product of sea ice concentration C and sea ice thickness H), where $D = -\nabla \cdot (\mathbf{u}V) = -\mathbf{u} \cdot \nabla V - V(\nabla \cdot \mathbf{u})$ represents dynamic processes. The first expression is the volume flux convergence, and this can be depicted in terms of minus the sum of advection and divergence (i.e., the two terms in the definition of D). A visual representation of these two terms is provided in Fig. S2. The last term (T) in the continuity equation represents thermodynamic processes, namely sea ice growth and melt, and is expressed as $T = \partial V/\partial t - D$. Budget components are calculated using a generalized budget analysis tool and processing script written in Python (https://github.com/CPOMUCL/Budget_tool).

The method of ice concentration and thickness tendencies to characterize thermodynamic and dynamic contributions to changes in sea ice concentration and volume has been implemented in a number of previous studies (Holland and Kwok 2012; Holland and Kimura 2016; Schroeter et al. 2018; Cai et al. 2020). In particular, Holland and Kwok (2012) examined budget terms contributing to the evolution in sea ice concentration, including the advection, divergence, and a residual term that combined both the thermodynamic and mechanical redistribution terms associated with ridging and rafting. Antarctic and Arctic observed ice concentration budgets were further examined using this approach in Holland and Kimura (2016). As is noted in an Antarctic sea ice volume budget assessment using CMIP5 simulations in Schroeter et al. (2018), using sea ice volume rather than concentration budgets allows the mechanical redistribution term to be incorporated into the change in sea ice thickness term so that the residual component is associated with actual sea ice growth/melt, namely thermodynamic contributions.

To compute the budget, we rely on PIOMAS daily effective thickness (Schweiger et al. 2011). Although NSIDC daily sea ice concentration (SIC) data from the NASA Team sea ice algorithm (Cavalieri et al. 1997) and produced in near-real-time from NSIDC (Fetterer et al. 2017) are not used for the budget analysis, they are presented to depict the spatial changes in SIC prior to, during, and following the 2012 and 2016 August storms. We use the PIOMAS daily effective thickness fields as there currently is no available sea ice thickness from satellites during summer months. The effective thickness H_{eff} is the equivalent thickness that one would obtain if all ice volume in the grid cell were evenly spread out including over open water, while in situ thickness is the ice floe thickness. While we recognize this is a modeled estimate of sea ice thickness, comparisons with observations from sonar on U.S. Navy submarines, mooring data, and satellite laser altimetry observations from *ICESat* showed generally good agreement (Schweiger et al. 2011). All data were regridded to the 25-km EASE-grid equal-area projection associated with the NSIDC sea ice drift fields (Tschudi et al. 2019).

Sea ice volume budget components in the vicinity of trajectories associated with extreme storms are derived based on interpolation of the storm tracks to EASE-grid and integration of volume budget components from 1 day prior to 1 day following the storm at each location.

Relative contributions to residual, thermodynamic, T, and dynamic, D [$\nabla \cdot (\mathbf{u}V)$], contributions are demonstrated via an index defined as

$$Q_{\text{td}} = (T^2 - D^2)/(T^2 + D^2).$$

In particular, $Q_{\text{td}} > 0$ indicates dominant contributions from thermodynamic processes, $Q_{\text{td}} < 0$ indicates dominant contributions from dynamic (advection and divergence) processes, and $Q_{\text{td}} \sim 0$ indicates comparable contributions from thermodynamic and dynamic processes. The index Q_{td} was also computed for adjacent grid cells based on the storm radius, to contrast the radius of influence between 2012 and 2016 (characterized by storms with larger area). Specifically, the index was computed at each grid cell located within the radius of influence during the storm (1 day prior to 1 day following), and the superposition of the Q_{td} for the radius of influence for all cyclones, as well as for the extreme cyclone (minimum SLP) shown. Cumulative impacts, in addition to two (binary) categories for Q_{td} indicating dominant thermodynamic and dynamic impacts of the storm on sea ice volume over the region of interest/radius of influence, are also identified.

$$D_f = \frac{|D|}{|D| + |T|},$$

$$T_f = \frac{|T|}{|D| + |T|}.$$

The relative fractional dynamic and thermodynamic changes in sea ice volume at each grid point prior to, during, and following extreme storms are additionally computed as $Q_{\text{thermo}} = T_f/(D_f + T_f)$ where $D_f = |D|/(|D| + |T|)$ and $T_f = |T|/(|D| + |T|)$. The index Q_{thermo} approaches values of 1 and 0 if the thermodynamic and dynamic processes govern, respectively. A value of 0.5 indicates that thermodynamic and dynamic processes are equally influential. Finally, the pan-Arctic change in SIA and volume is computed as the slope for each following the onset of the 2012 and 2016 storms.

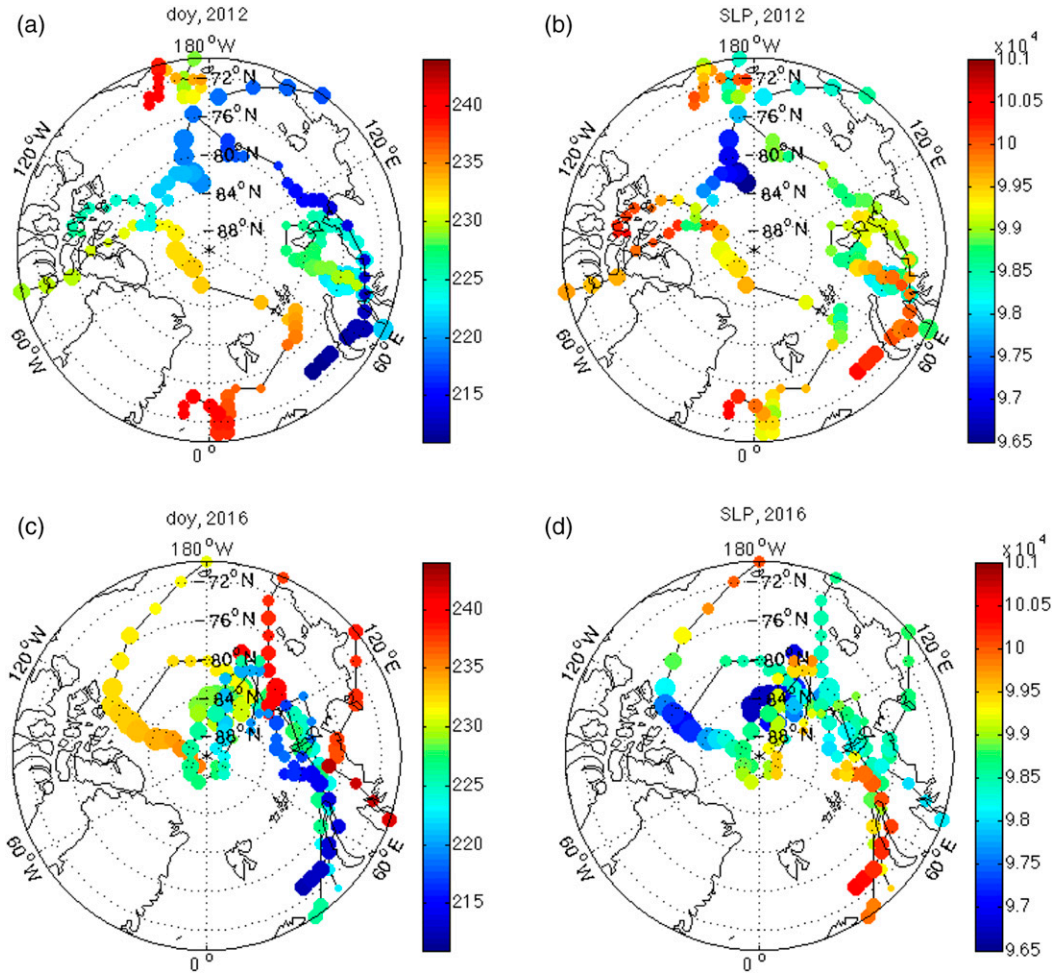

FIG. 2. Trajectories associated with extreme cyclones from 1 to 30 August, with colors depicting (a),(c) day of year and (b),(d) SLP in hPa in (top) 2012 and (bottom) 2016.

Budget closure

To address the issue of closure associated with combining reanalysis and observational data, we examine the method of Mayer et al. (2018) to create a product that blends the NSIDC drift product with PIOMAS drift data. Specifically, the method of Lagrange multipliers outlined in Mayer et al. (2018) and designed to minimize discrepancies associated with combined datasets is implemented to create adjusted budget terms F^a from the original budget terms, namely those generated using the PIOMAS effective thickness and NSIDC drift product without buoy data combined F' such that

$$F_i^a = F_i' + \frac{\sigma_i'^2}{\sum_k \sigma_k'^2} \cdot \Delta,$$

where $F_i' \equiv (D_{\text{adv}}, D_{\text{div}}, T)$ includes the dynamic (advection and divergence) and thermodynamic terms, respectively, σ_i' depicts the standard deviation among the NSIDC (with and without buoy data) and PIOMAS sea ice drift products for the budget term F_i', and Δ refers to residual or the difference between the PIOMAS and NSIDC-generated budget terms resulting from differences in the drift product. The index k runs over all budget terms. Both version 4, with assimilated buoy data (Tschudi et al. 2019), and a modified version without the buoy data (provided by Scott Stewart and NSIDC), are included in the analysis. However, caution is needed when using the product with assimilated buoy data as the merging of buoy and satellite data affects spatial gradient calculations.

3. Results

We begin with a characterization of the cyclone trajectories and strength in August 2012 and 2016, before turning our attention to changes in the ice cover and decomposition of the volume budget. In the volume budget figures that follow, positive divergence terms represent convergence, while positive advection terms indicate that thicker ice moves into the region in the direction of motion. Conversely, when the

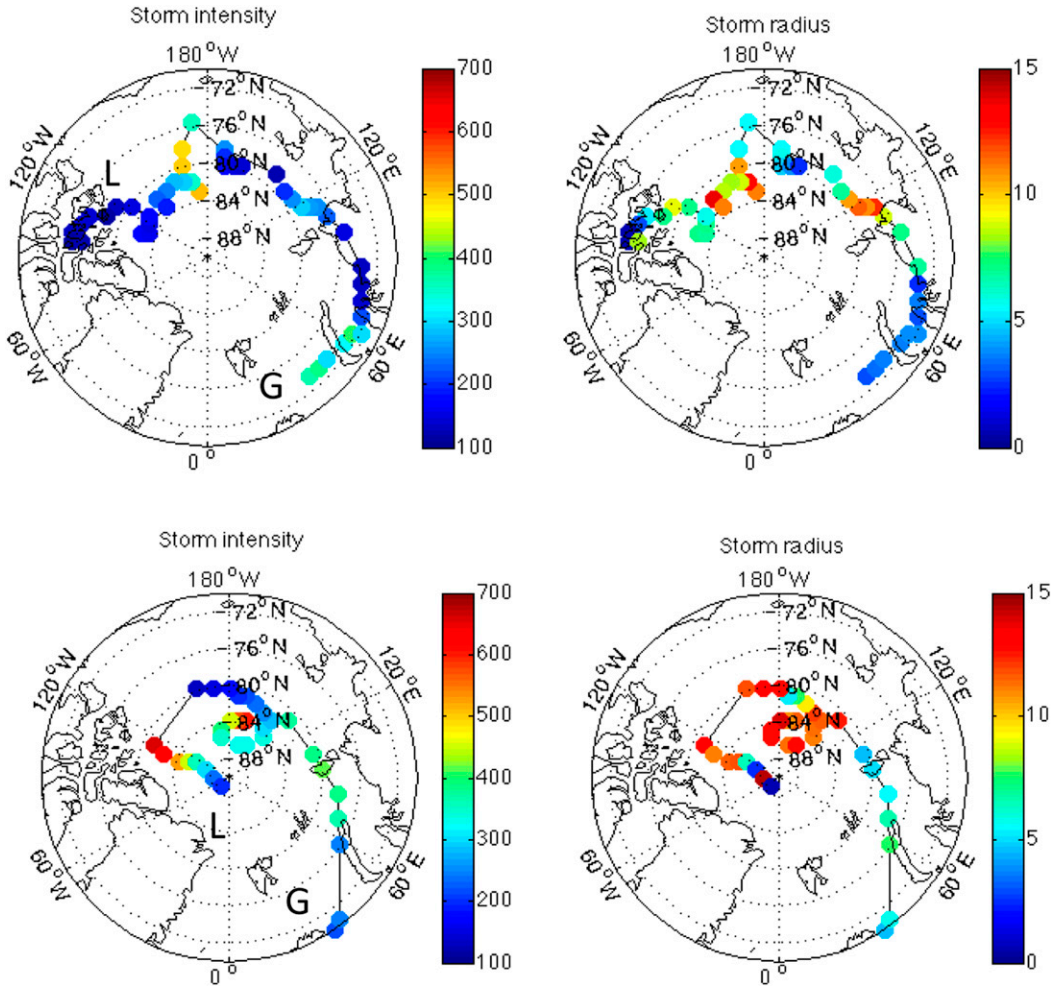

FIG. 3. Extreme cyclone trajectory characteristics in (top) 2012 and (bottom) 2016 with colors depicting (left) storm intensity [in Pa $(10^4\,\mathrm{km}^2)^{-1}$] and (right) storm radius (in 10^2 km). Genesis and lysis points are indicated by letters G and L, respectively.

advection term is negative, thinner ice has moved into the grid cell in the direction of motion.

a. Distribution and timing of extreme storms

In both 2012 and 2016, several extreme cyclones occurred in August. The Great Arctic Cyclone of 2012 was found to be influenced by baroclinicity and the tropopause polar vortex (Simmonds and Rudeva 2012), whereas the August 2016 cyclone was attributed to baroclinicity and a merging of/coherence in upper- and lower-level warm cores (Yamagami et al. 2017). Trajectories associated with extreme storms in August 2012 originate over the Arctic Atlantic sector and Siberia in early August and via Bering Strait in late August (Fig. 2a), while in 2016 trajectories originate in the Atlantic Ocean and Barents Sea in early August, and over Siberia in late August (Fig. 2c). In 2012, the SLP minimum on 6 August (day of year 219) is located near 83°N, 173°W, with a value of ~964 hPa (Fig. 2b). In 2016, two SLP minima are observed over the central Arctic (Fig. 2d); the SLP minimum on 16 August (day of the year 229) is located farther north, near 85°N, 171°W, with a value of ~967 hPa, while a secondary SLP minimum on 20 August (day of year 233) is located farther south near 81°N, 114°W, with a value of ~971 hPa. The existence of two SLP minima over the central Arctic in 2016 reflects the merging of two storms originating from the Atlantic and Pacific sectors; in this study we focus on the extreme storm of Atlantic origin since it is associated with the SLP minimum.

Further characterization of the 2012 and 2016 most extreme Arctic storms according to intensity and radius (Fig. 3) shows that in 2012, the storm was most intense 12 h earlier than the SLP minimum, near 82°N, 168°W, with a radius on the order of 1100 km. The storm's largest radius (approximately 1400 km) occurred on 8 August 2012, with the majority of days having radius values less than 1000 km. In 2016, the storm was most intense on 20 August, with a secondary SLP minimum near 81°N, 150°W and a radius of ~1300 km. On 22 August, the radius of the storm was at its largest, with a radius of

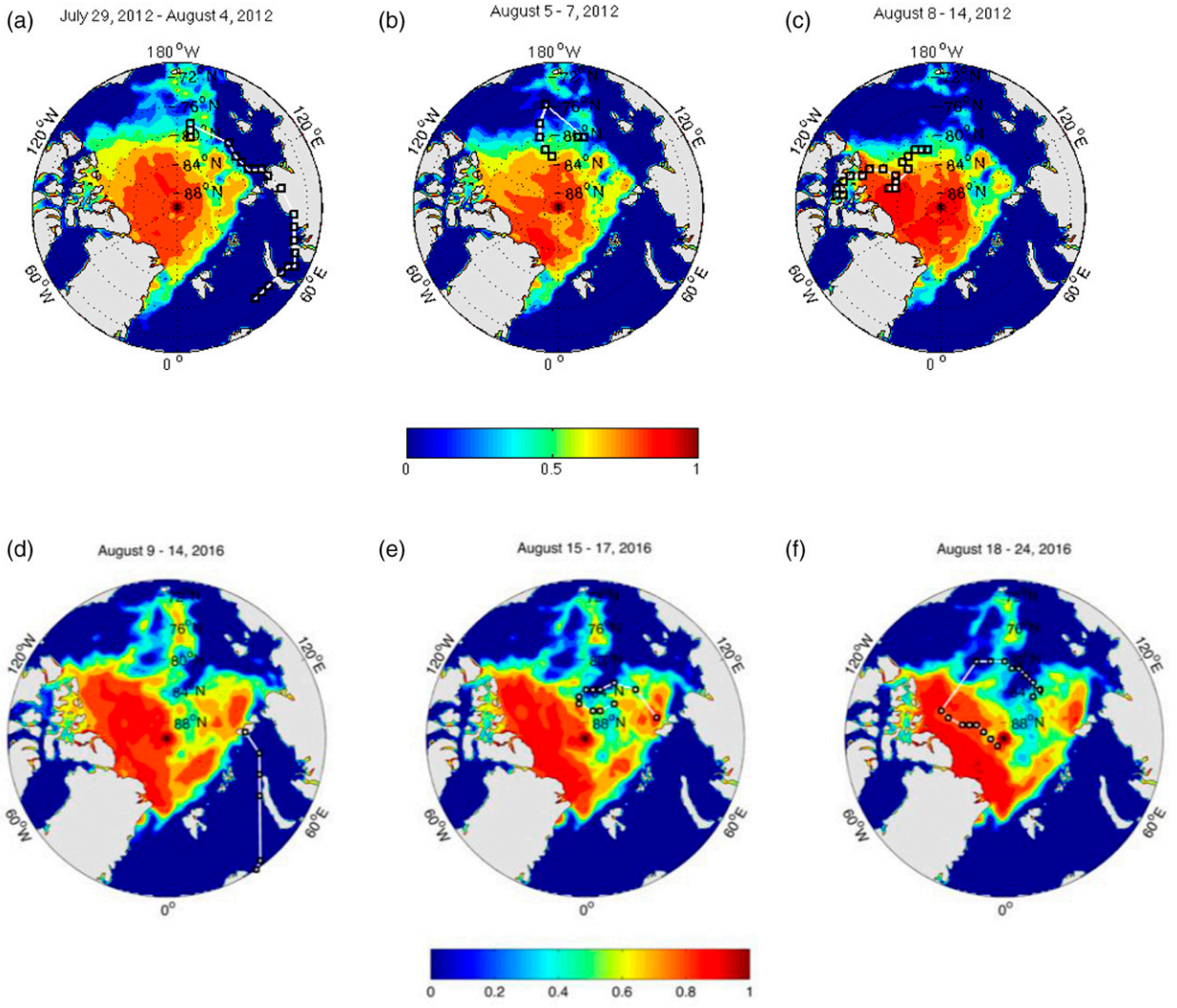

FIG. 4. NSIDC sea ice concentration (SIC) maps and ERA-Interim SLP minimum/extreme cyclone trajectories prior to, during and following extreme storm event for (a) 29 Jul–4 Aug, (b) 5–7 Aug, and (c) 8–14 Aug 2012 and for (d) 9–14 Aug, (e) 15–17 Aug, and (f) 18–24 Aug 2016.

approximately 1450 km although in contrast to 2012, the minimum SLP trajectory in 2016 typically exceeded a radius of 1000 km. This had important implications for nonlocal storm impacts on sea ice and advection, as shown later.

In consideration of our first research question, namely the spatial distribution and timing of all August storms in 2012 and 2016, cyclone trajectories from 1 to 30 August show an equatorward displacement in cyclone trajectories in early August 2012 relative to 2016, and an accumulation of trajectories over the central Arctic in mid-August 2016 (Figs. S3 and S4). Storms enter the Arctic Atlantic and Pacific sectors in early August in 2012, and the central Arctic and Atlantic sector in mid-to-late August in 2016.

Sea ice conditions (concentration, effective thickness, and drift) prior to, during, and following the most extreme Arctic cyclones of 2012 and 2016 demonstrate differences in regional and local storm impacts on Arctic sea ice (Figs. 4–6). In 2012, high SIC exists over the central Arctic and values of approximately 50% are observed in the Pacific sector before the 6 August storm (Fig. 4a). SIC is then reduced to ~80% in the central Arctic and nearly vanishes in the Pacific sector (in the vicinity of the cyclone) during the extreme storm (Fig. 4b). Subsequent recovery of SIC to approximately 100% occurs in the central Arctic (most likely associated with refreezing). Sea ice loss continues in the Pacific sector following the storm (Fig. 4c). In 2016, SIC is also high in the central Arctic before the 16 August storm (Fig. 4d). However, SIC is enhanced to ~99% north of the Canadian Arctic Archipelago (CAA) as sea ice converges and is compressed against the shoreline in response to the merging of two storms, while SIC falls in the vicinity of storms near 84°N during the storm (Fig. 4e). In the following period, SIC increases (decreases)

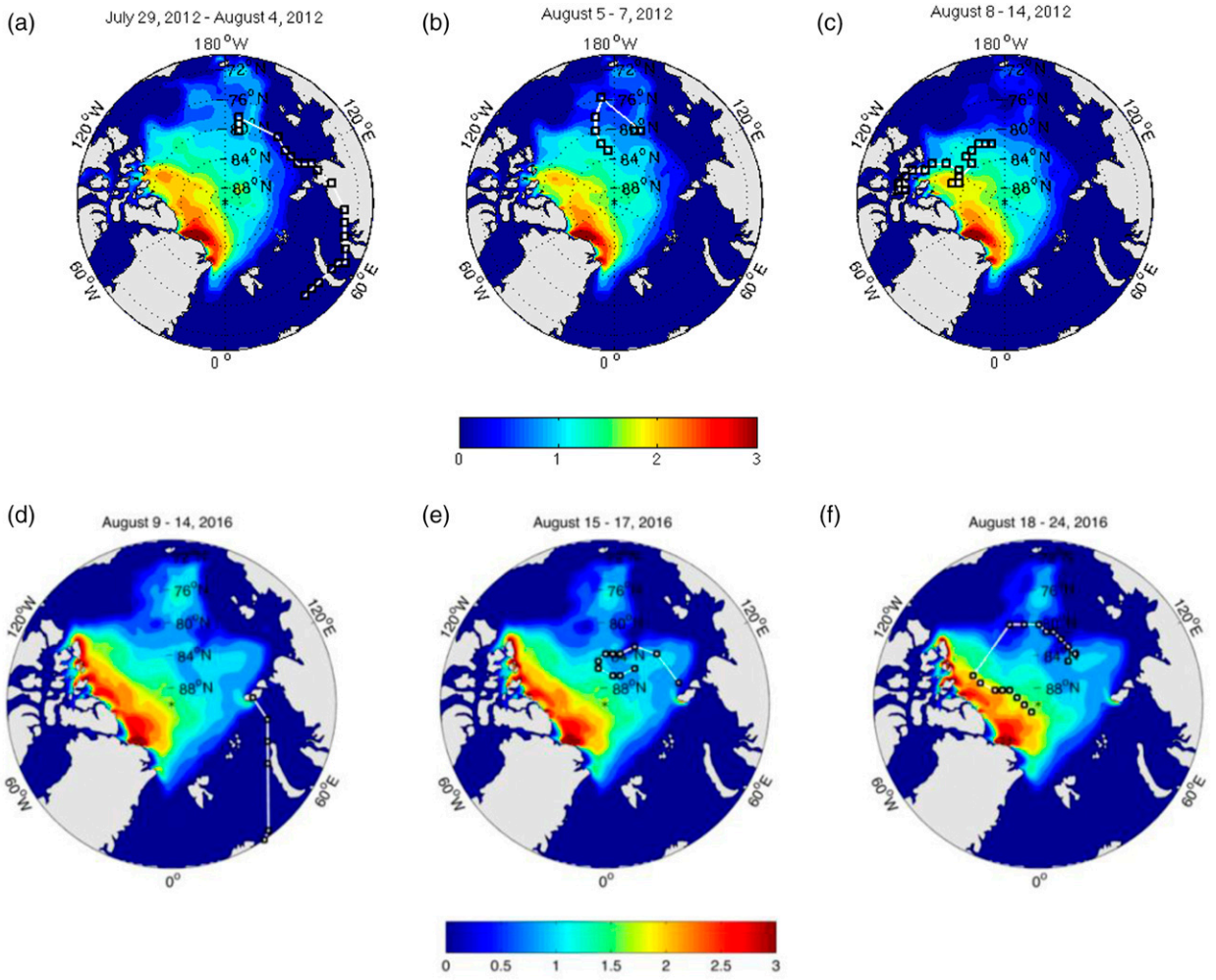

FIG. 5. PIOMAS effective sea ice thickness maps (in m) and ERA-Interim SLP minimum/extreme cyclone trajectories prior to, during, and following extreme storm event for (a) 29 Jul–4 Aug, (b) 5–7 Aug, and (c) 8–14 Aug 2012 and for (d) 9–14 Aug, (e) 15–17 Aug, and (f) 18–24 Aug 2016.

poleward (equatorward) of the storms located over the central Arctic (Fig. 4f).

PIOMAS-modeled H_{eff} in 2012 suggests the ice thickness was less than 1 m in the Pacific sector prior to the storm arriving, and values north of the CAA and Greenland ranged from 2 to 3 m (Fig. 5a). During the 6 August storm, significant thinning of ice occurred in the Pacific sector in the vicinity of the storm near the sea ice edge, with a slight thinning north of the CAA (Fig. 5b). Following the storm there was sustained thinning in the Pacific sector and in the vicinity of storms north of the CAA (Fig. 5c). In 2016, H_{eff} is characterized by a coherent band of 2–3-m-thick ice north of the CAA and Greenland and ~1.5-m-thick ice near the ice edge/periphery before the 16 August storm (Fig. 5d). During the storm, sea ice thinned slightly in the vicinity of storms in the central Arctic (Fig. 5e), and sea ice thinning occurred in the Atlantic sector following the 16 August storm (Fig. 5f).

Further, distinctive differences in sea ice response to storms in 2012 and 2016 are evident in sea ice drift fields (Fig. 6). Before the 6 August storm in 2012, weak cyclonic circulation in the Beaufort Sea and advection in Fram Strait is observed (Fig. 6a). In response to the 6 August storm and cyclonic circulation near the sea ice edge, sea ice drift is enhanced along the sea ice edge in the Beaufort Sea (within the reduced SIC and thickness regime in the Pacific sector) and north of the Laptev Sea (Fig. 6b). The dissipated sea ice cover disappears in the Pacific sector and sustained enhanced cyclonic (southeastward) drift is observed in the low ice concentration regime of the Beaufort Sea in response to storms as they migrate to the CAA following the 6 August event (Fig. 6c). In 2016, cyclonic sea ice circulation is observed north of Greenland prior to the 16 August extreme storm (Fig. 6d), which is enhanced during 15–17 August in response to two cyclones migrating over the central Arctic including the 16 August extreme storm (Fig. 6e). Remnants of enhanced drift exist for ~1-m-thick ice north of Bering Strait and 1.5-m-thick ice in the eastern Beaufort Sea and over the central Arctic, as well as north of the CAA and

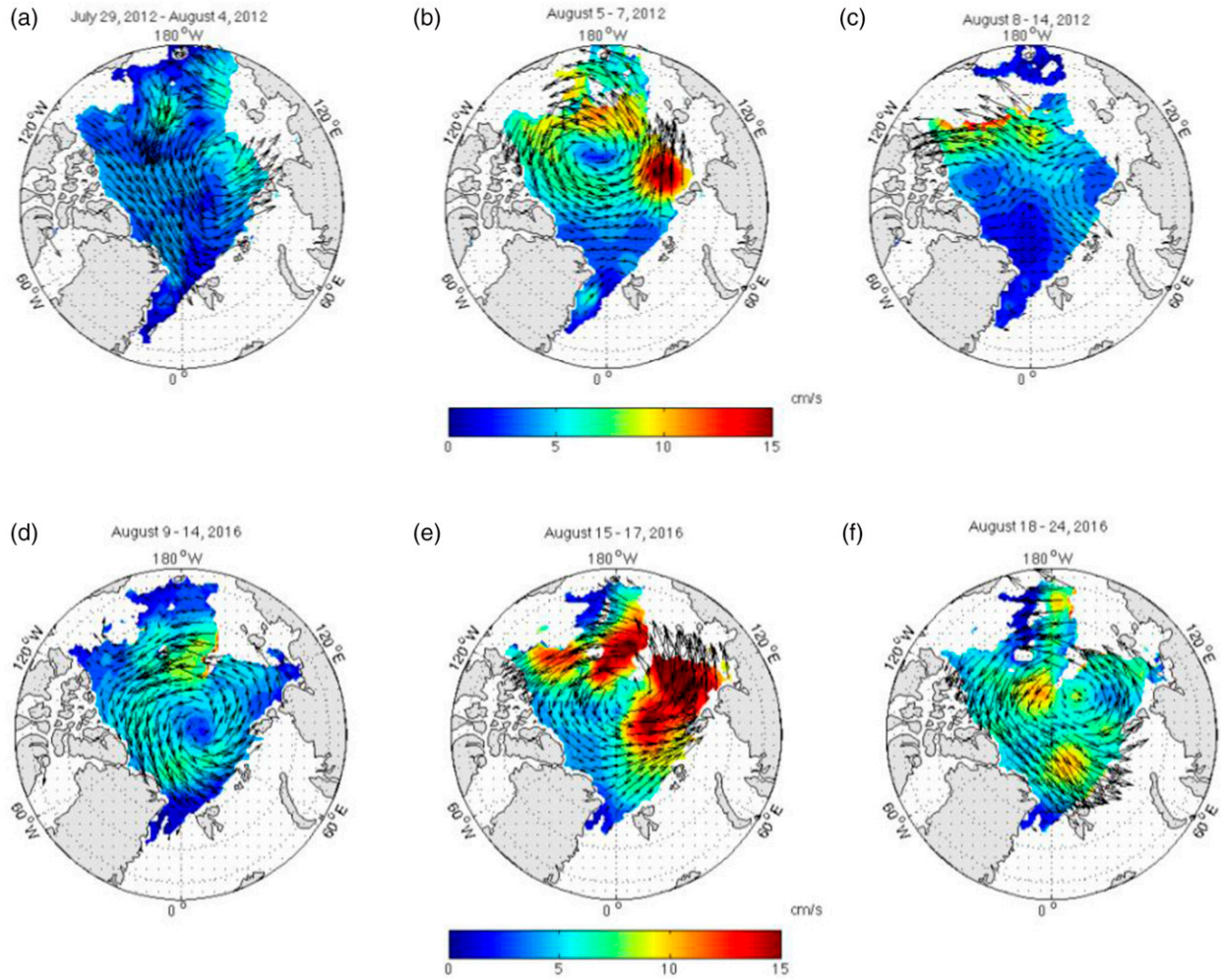

FIG. 6. NSIDC sea ice drift (without buoy data) maps (in cm s^{-1}) and ERA-Interim SLP minimum/extreme cyclone trajectories prior to, during, and following extreme storm event for (a) 29 Jul–4 Aug, (b) 5–7 Aug, and (c) 8–14 Aug 2012 and for (d) 9–14 Aug, (e) 15–17 Aug, and (f) 18–24 Aug 2016.

Greenland as cyclones continue to traverse the central Arctic following the 16 August 2016 extreme storm (Fig. 6f). Noteworthy is enhanced drift at the periphery of the ice pack in 2012, and over the central Arctic in 2016. Enhanced drift is in keeping with a weaker ice cover as documented by Parkinson and Comiso (2013) and Zhang et al. (2013) for the 2012 minimum SIE, and low compactness as documented by Petty et al. (2018) for 2016.

b. *Thermodynamic and dynamic influences*

The above analysis already hints at some distinct differences in impacts on the ice cover from the August 2012 and 2016 extreme cyclones. Decomposition of the sea ice volume change (or thickness change) helps to quantify the thermodynamic versus dynamical influences (Figs. 7 and 8, in addition to Figs. S5 and S6). Figures 7 and 8 depict the volume budget components computed using PIOMAS H_{eff} and NSIDC (without buoy data) sea ice drift, while Figs. S5 and S6 depict adjusted volume budget components using the method of Lagrange multipliers previously described to address the budget closure issue, in addition to storm trajectories. (The standard deviation for the adjusted residual term, depicted in Fig. S10, provides a measure of the uncertainty associated with the use of all three sea ice drift products and, once summer thickness observations are available from NASA's *ICESat-2*, can be used in model–observational data comparisons to evaluate model performance in characterizing storm impacts on sea ice). As is evidenced by similarity in the intensification and residual components, the intensification rate a week prior to the 6 August 2012 extreme storm is governed by reductions in sea ice volume due to melt throughout the Arctic, except the region northeast of Greenland, which is characterized by sea ice growth (top rows of Fig. 7 and Fig. S5). During the storm (centered on 6 August), changes in sea ice volume were primarily a result of increased thermodynamic melt (middle rows of Fig. 7 and Fig. S5), with sea ice volume loss and divergence near the sea ice edge in the

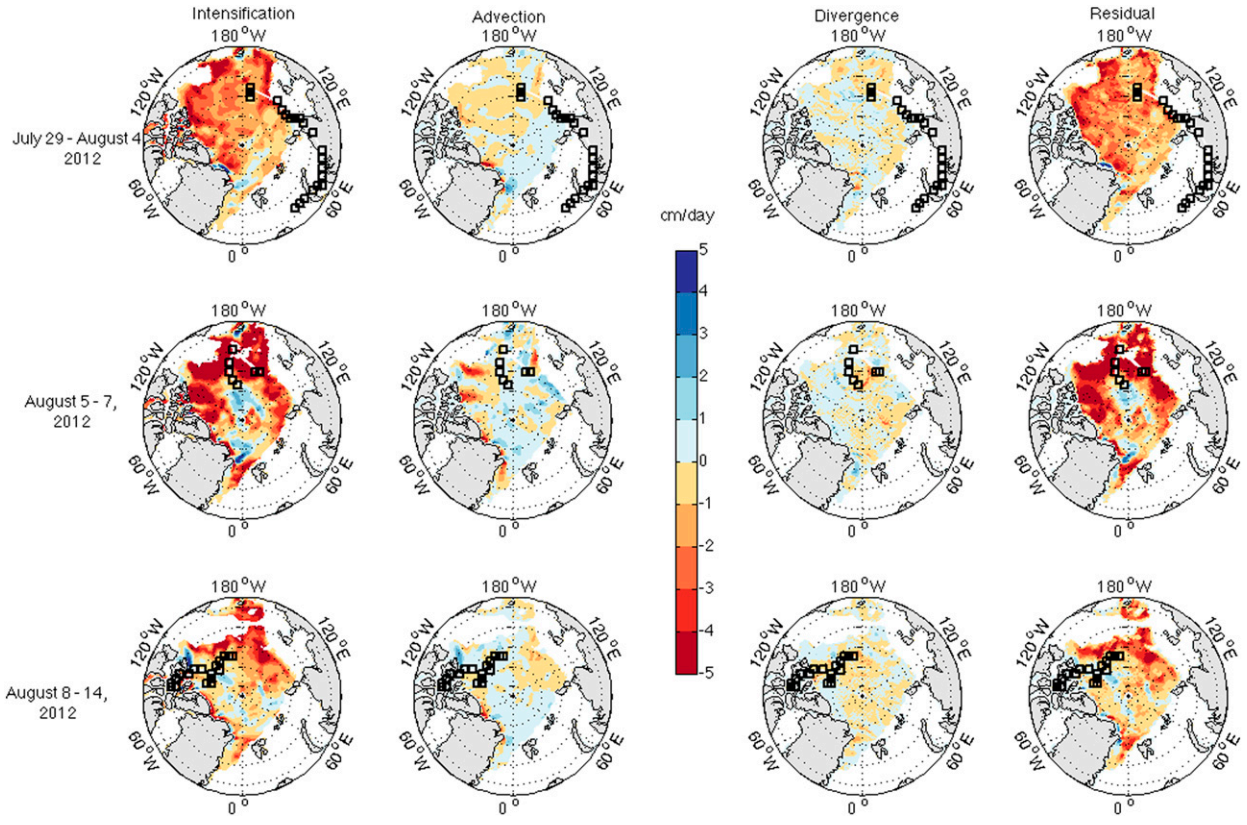

FIG. 7. Sea ice volume budget components including (left to right) intensification, advection, divergence, and residual terms (top) prior to, (middle) during, and (bottom) following the 6 Aug 2012 extreme storm, computed using PIOMAS effective thickness and NSIDC sea ice drift. Units are cm day^{-1}. Blue (red) values indicate sea ice volume increase (decrease).

Pacific sector. An increase in ice volume, by contrast, was found in the central Arctic north of the CAA and Greenland due in part to the advection of thicker ice into the area. After the storm passed, changes in sea ice volume from 8 to 14 August are governed by sea ice loss in the Pacific sector that extends north of the Laptev Sea, growth north of the CAA and Greenland, and contributions near the sea ice edge from sea ice melt and to a lesser extent advection of thinner ice into the Beaufort Sea region (bottom rows of Fig. 7 and Fig. S5).

In 2016, before the 16 August storm hit, overall ice volume changes a week before the storm were more modest than in 2012, with changes in sea ice volume from 9 to 14 August characterized by increases north of Greenland and decreases in the central and Pacific sector of the Arctic associated with the thermodynamic component, in addition to increases to the northeast of Greenland associated with the dynamic component (advection and convergence; top rows of Fig. 8 and Fig. S6). During the 16 August storm, sea ice volume increase north of the CAA and Greenland is suppressed due to the advection of thicker ice out of the region, weakened convergence, and melt; sea ice volume decreases near the sea ice edge north of the Beaufort Sea due to advection of thinner ice into the region and melt (middle rows of Fig. 8 and Fig. S6). Interestingly, following the 2016 storm, continued volume reduction is observed north of the CAA, while an increase is observed north of Norway due to advection of thicker ice into the region (bottom rows of Fig. 8 and Fig. S6). This is in contrast to conditions following the 2012 storm and may reflect differences in the timing and the size of the storms that entered the region in mid-to-late August in 2016. Noteworthy is the aforementioned presence of two storms in the central Arctic, in addition to enhanced advection in 2016 relative to 2012 due to larger spatial extent of the 2016 storms, with nonlocal implications. As is noted in Yamagami et al. (2017), continued volume reduction following the 2016 storm may also be attributed to multiple merging of Arctic and midlatitude storms throughout the month of August 2016.

Fractional dynamic and thermodynamic contributions (Q_{thermo}, computed as the ratio of the absolute value of each to their sum) to changes in sea ice volume illustrate dynamic contributions in the central Arctic and thermodynamic contributions (exceeding 80%) in the Pacific sector and near the sea ice edge during the 6 August 2012 storm (Fig. 9). Following the storm, dynamic contributions (~50%–60%) are observed north of the Beaufort Sea in the vicinity of the storm cluster, with predominantly thermodynamic contributions elsewhere. In 2016, dominant dynamic contributions (exceeding 80%) are observed in the central Arctic north of Greenland and north of the Laptev and East Siberian Seas during the extreme 16 August storm (Fig. 10), while comparable dynamic and thermodynamic

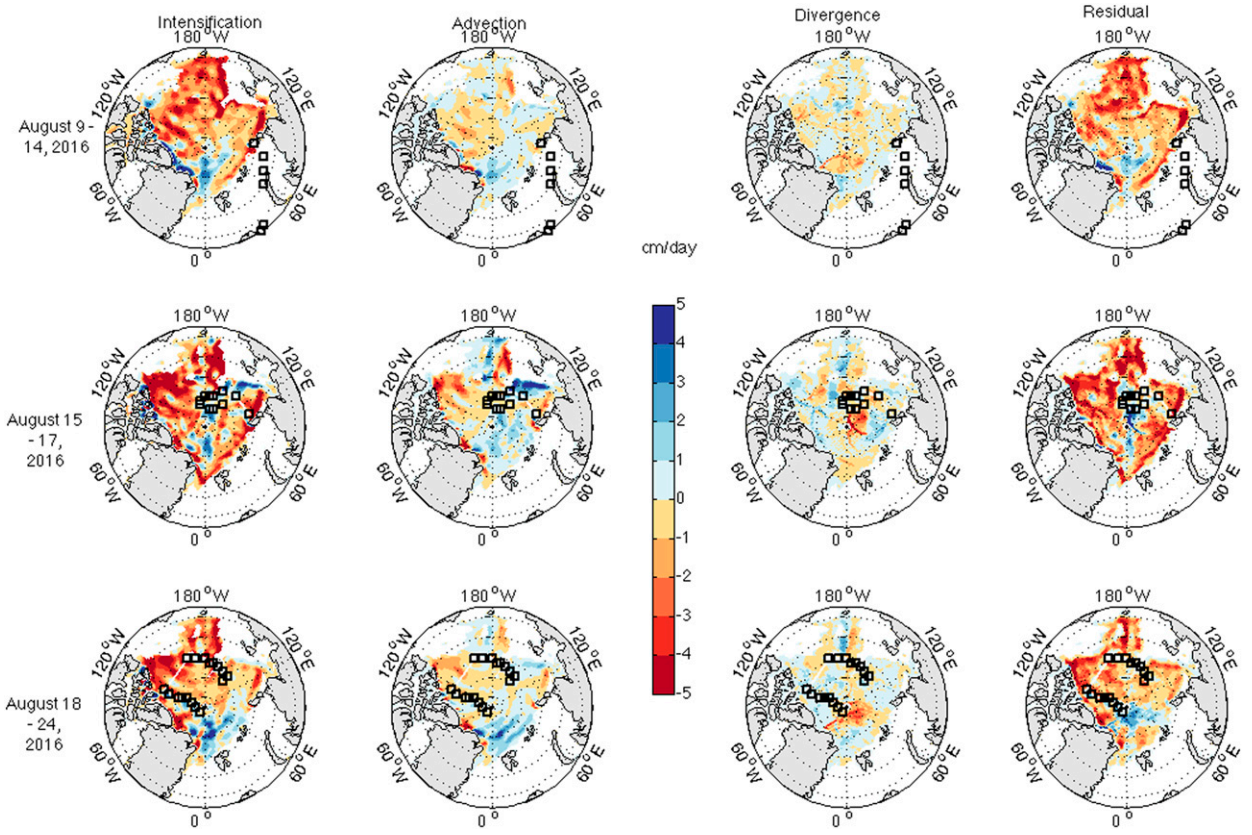

FIG. 8. Sea ice volume budget components including (left to right) intensification, advection, divergence, and residual terms (top) prior to, (middle) during, and (right) following the 16 Aug 2016 extreme storm, computed using PIOMAS effective thickness and NSIDC sea ice drift. Units are cm day^{-1}.

contributions (~50%) interspersed among dominant thermodynamic contributions are observed throughout the Arctic following the storm. This provides a signature of nonlocal contributions from larger storms in 2016 relative to 2012. Whereas 2012 is characterized by predominantly thermodynamic storm impacts on sea ice volume in the Pacific sector, 2016 is characterized by dynamical storm impacts on sea ice volume throughout the Arctic (due to storm timing and location).

Turning to local-scale impacts, volume budget components in the vicinity of storms are summarized by the Q_{td} index (Fig. 11). Positive index values, characteristic of thermodynamic contributions, are observed in the Pacific sector near the ice edge and region of significant ice loss in 2012 (left column of Fig. 11). However, negative values, characteristic of dynamic contributions, are also observed in the northern Canada Basin and in the thick sea ice regime north of the CAA and Greenland, interspersed with thermodynamic contributions. Comparison with 2012 volume budget components (Fig. S7) shows sea ice accumulation in the northeastern Canada Basin due to advection of thicker ice into the region near the coast, advection and divergence (which cancel) and sea ice growth farther offshore, convergence north of the Canada Basin, and divergence when the storm is at maximum intensity. Furthermore, convergence and advection contribute to dynamic changes in sea ice volume in this region as ice is compressed against the coastline. In 2016, storm impacts on sea ice are characterized by combined thermodynamic and dynamic contributions over the central Arctic [and predominantly dynamic contributions north of the Laptev Sea] (right column, Fig. 11). The spatial distribution of superimposed Q_{td} values for cyclone radii (top row of Fig. S8) highlights thermodynamic contributions in the Pacific sector near the sea ice edge in 2012, and interspersed with dynamic contributions in the vicinity of storms north of the Laptev and East Siberian Seas and over the central Arctic in 2016. Examination of Q_{td} values within the radius of the extreme storm associated with the SLP minimum (lower row, Fig. S8) further demonstrates predominantly thermodynamic contributions in the Pacific sector in 2012, and dynamic nonlocal and local contributions to volume changes at the sea ice edge/periphery and central Arctic in 2016. These broad conclusions are further supported by the cumulative Q_{td} values (middle row of Fig. 11) and further reflected in the binary, or two-category, assessment of cumulative thermodynamic and dynamic contributions to changes in sea ice volume along the extreme storm trajectory (bottom row of Fig. 11).

Does the thermodynamic term, calculated as the residual, provide a realistic estimate of melt/growth rates? Previous studies document melt rates on the order of 0.5 cm day^{-1} in the central Arctic observed during the SHEBA campaign (Perovich

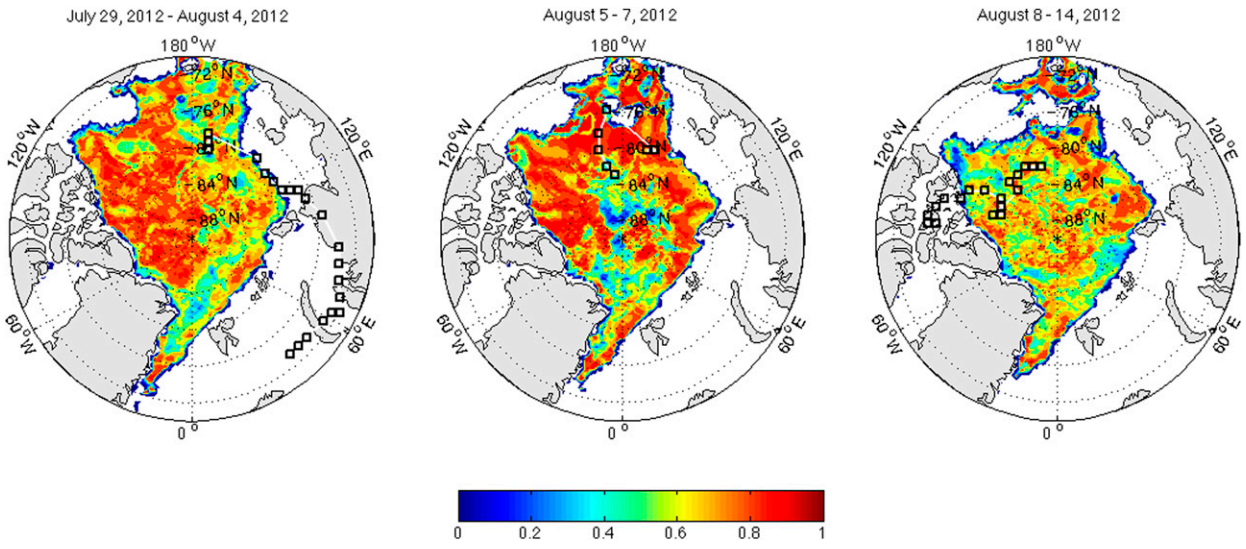

FIG. 9. Fraction of thermodynamic and dynamic contributions to sea ice volume changes (left) before, (middle) during, and (right) following the 6 Aug 2012 extreme storm. Red (blue) shading indicates dominant thermodynamic (dynamic) contributions.

et al. 2003), while an assessment of regional variability based on summertime ice mass balance (IMB) measurements record values on the order of 1.5 cm day^{-1} for the 2000–14 timeframe (Perovich and Richter-Menge 2015). More recently, West et al. (2019) found melt rates ranging from 2 to 6 cm day^{-1} before and during the 2012 extreme storm in Fram Strait, while Lei et al. (2020) found basal melt rates on the order of 2.2 cm day^{-1} in August 2016 in the IMBs, and if surface melt is on the order of 0.5 cm day^{-1}, this implies total melt rates of ~3 cm day^{-1}. Even higher melt rates are recorded north of Svalbard in response to storms (Duarte et al. 2020), with values of 6–9 cm day^{-1} for 1-m-thick floes, and twice that rate for 2-m-thick floes.

In consideration of simulated melt rates, Cai et al. (2020) provide estimates of thermodynamic contributions to changes in sea ice thickness in response to storms using CMIP5 models and find thermodynamic values of up to 5 cm day^{-1}. Furthermore, Tsamados et al. (2015) provided estimates for simulated top, basal, and lateral melt and investigated the relative contributions of each to total melt based on the CICE sea ice model, with values in August on the order of 0.5, 1.5, and 0.2 cm day^{-1}, respectively. Recorded and simulated melt rates (Figs. S11 to S17), ranging from 2 to 6 cm day^{-1}, with enhanced rates during extreme storms, are consistent with values found for the residual/thermodynamic term in the

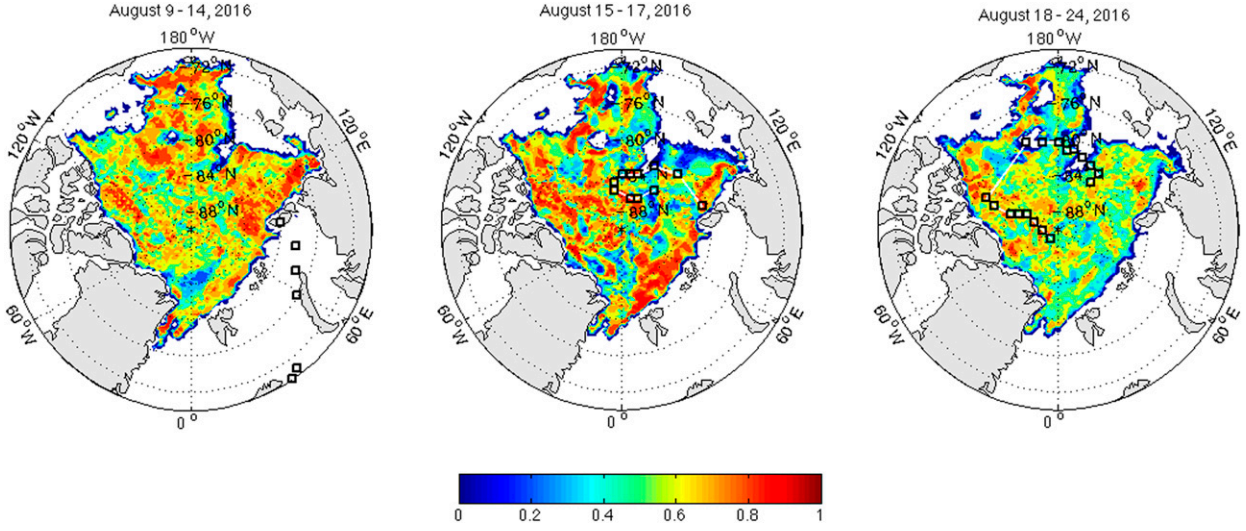

FIG. 10. As in Fig. 9, for the 16 Aug 2016 extreme storm.

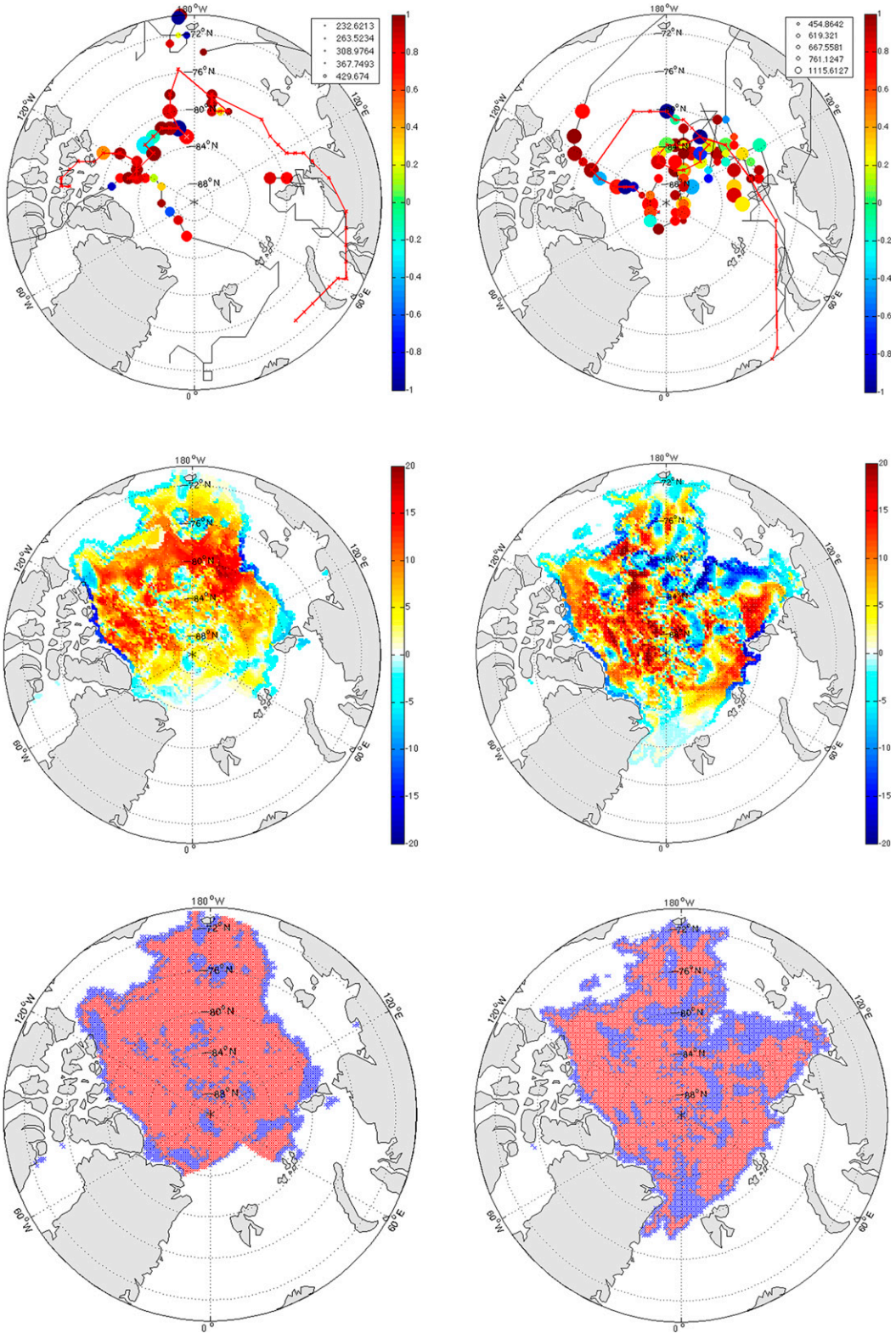

FIG. 11. (top) Thermodynamic/dynamic index Q_{td} for storms along extreme storm trajectories for 2012 and 2016 with no filter applied. Symbol size depicts variations in storm intensity. Cumulative thermodynamic/dynamic index Q_{td} for storms along and surrounding extreme storm trajectories for (left) 2012 and (right) 2016. (middle) The cumulative value for Q_{td} at each grid point impacted by cyclones along the extreme storm trajectory. (bottom) A binary interpretation of cumulative thermodynamic (red) and dynamic (blue) contributions to changes in sea ice volume also along the extreme storm trajectory.

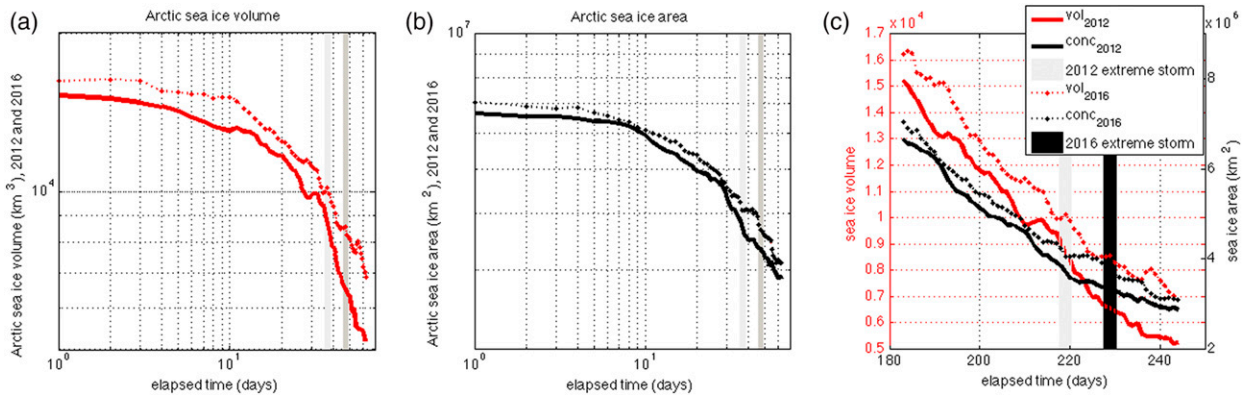

FIG. 12. Time series for Arctic sea ice (a) volume, (b) area, and (c) volume (red) and area (black) for 2012 (solid line) and 2016 (dashed line). Elapsed time indicates days from 1 Jul (day of year 183). Vertical bars indicate the 6 Aug 2012 (light) and 16 Aug 2016 (dark) storms. Note that (a) and (b) are depicted on a log–log scale to highlight slopes following storms.

present study (Figs. 7 and 8). Thus, past findings based on simulated and observed melt rates support interpretation of the residual as the thermodynamic term and a realistic representation of melt/growth rates in the Arctic.

c. *Storm impact on Pan-Arctic sea ice cover*

How did these storms impact the overall pan-Arctic sea ice cover and hence the ability to forecast the sea ice minimum? Pan-Arctic decline in SIA in both years was broadly similar (Fig. 12b), whereas there was a faster decline in ice volume in 2012 relative to 2016, evident in a steeper slope following the 6 August 2012 storm (Fig. 12a). The transition in the sea ice volume and concentration decay during the 2012 extreme storm is consistent with the modeling study of Zhang et al. (2013). Following the 2012 storm, sea ice volume loss accelerates, while SIA decays less rapidly (Fig. 12c). By contrast, the SIA and volume decay slopes following the 2016 extreme storm are comparable, reflecting the impact of storms located over the central Arctic on thicker ice north of the CAA. Pan-Arctic changes in SIA following the onset of the extreme storms are 5.0×10^4 and 5.5×10^4 km^2 day^{-1} in 2012 and 2016, respectively (Table 1). The rate of pan-Arctic ice volume loss following the 2012 storm (207.5 km^3 day^{-1}) is approximately 4 times what was encountered following the 2016 storm (56.2 km^3 day^{-1}). It should be noted that these values may also reflect a seasonal signal and nonlinearity in ice melt since both storms occur on different days of the year; of interest however are relative changes in SIA and volume for both years. Pan-Arctic changes in SIA and volume during storms highlight abrupt change in the 2012 in contrast to the 2016 extreme storm. Results are insensitive to spatial scale (see Fig. S9 and description in the online supplemental material).

The present study indicates enhanced volume loss in 2012 (207.5 km^3 day^{-1}) relative to 2016 (56.2 km^3 day^{-1}) and higher rates both during and following extreme storms than those documented in earlier studies. Differences between the volume loss rates in 2012 and 2016 can be attributed to storm timing and location. In 2012 the passage of the extreme storm track over the Pacific sector of the Arctic resulted in significant melt evident in the thermodynamic response. By contrast, in 2016 the passage of the extreme storm track over the central Arctic resulted in a thermodynamic and counteracting dynamic response that would inhibit ice melt. Differences in 2012 and 2016 SIA rates of change relative to past studies may be attributed to enhanced loss in the Pacific sector due to melt of a thinner ice cover in 2012, as well as enhanced storm area and thus nonlocal impacts on a thinner and more mobile ice cover in 2016.

4. Discussion and implications

While it remains uncertain how Arctic cyclone intensity and frequency will change in the future (Akperov et al. 2015; Crawford and Serreze 2017; Day et al. 2018), a thinner and weaker ice cover will become more responsive to extreme cyclone events. Previous modeling studies of storm impacts on sea ice

TABLE 1. Changes in pan-Arctic sea ice area and volume following onset of extreme storm (1 day prior to 8 days following extreme storm) and during extreme storm (2 days prior to 2 days following extreme storm).

	Pan-Arctic change in sea ice area following onset of extreme storm (km^2 day^{-1})	Pan-Arctic change in sea ice volume following onset of extreme storm (km^3 day^{-1})	Pan-Arctic change in sea ice area during extreme storm (km^2 day^{-1})	Pan-Arctic change in sea ice volume during extreme storm (km^3 day^{-1})
2012	-5.0×10^4	−207.5	-9.3×10^4	−217.7
2016	-5.5×10^4	−56.2	-3.8×10^4	−87.0

(Semenov et al. 2019) showed that intense storms in the Arctic North Atlantic generate a low pressure system in the Kara Sea that with a thinner and more mobile ice cover enhances ice export via Fram Strait (e.g., Rampal et al. 2009). On the other hand, intense storms in the Arctic North Pacific sector generate a low pressure system in the Chukchi Sea that inhibits ice transport from the Canada Basin and north of the Canadian Archipelago to the Beaufort and Chukchi Seas. Additionally, thermodynamic processes characterized by net sea ice heat fluxes were shown to contribute to enhanced sea ice loss in the east Greenland and southern Beaufort Seas in response to storms (Semenov et al. 2019). Kwok (2006) noted that correspondence between sea ice divergence and large-scale sea ice vorticity will increase over a range of (smaller) spatial scales as the ice cover continues to thin. Present results confirm this hypothesis and corroborate what was initially documented for summer 2002 by Serreze et al. (2003), who noted that cyclonic circulation gives rise to sea ice divergence and rapid melt; similar behavior is observed near the sea ice edge in 2012 (resulting in accelerated sea ice loss in the Pacific sector of the Arctic), and to a lesser extent in the central Arctic in 2016.

Results from the present study are also consistent with previous studies that have investigated individual storm impacts on summer Arctic sea ice concentration. In particular, Kriegsmann and Brümmer (2014) found sea ice concentration (SIC) loss at cyclone centers that is amplified by deformation in response to increased storm intensity, both elements of which contribute to an overall acceleration in sea ice melt in summer. Similarly, Schreiber and Serreze (2020) found an increase in SIC reduction in the central Arctic and decrease in SIC reduction in coastal regions in response to storms in summer. In our study, the intensification and residual (thermodynamic) sea ice volume budget components similarly show enhanced sea ice melt and reduction in sea ice thickness in response to the August 2012 and 2016 extreme cyclones (Figs. 7 and 8), while further demonstrating local and regional changes in sea ice thickness in response to storm timing and location.

Turning back to the issue of forecasting sea ice conditions a few months in advance, current limitations are evident by the unexpected differences between observed and July predictions of September SIE, in addition to recognition of the increasingly important role played by extreme Arctic cyclones in contributing to accelerated summertime sea ice loss due to divergence and enhanced lateral/basal melting (Zhang et al. 2013; Graham et al. 2019). Reduced predictability highlights the need for improved understanding of extreme storm impacts on sea ice volume from a scientific perspective, and on planning, preparedness, and forecasting skill from a societal perspective.

5. Conclusions

Results from this analysis demonstrated that thermodynamic and dynamic contributions to ice volume loss in 2012 and 2016 were governed by extreme cyclone location and timing in summer. Considering our first research question, cyclones enter the Arctic Atlantic and Pacific sectors in early August in 2012, and the central Arctic and Atlantic sector in mid- to late August in 2016. In 2012 and 2016 extreme Arctic cyclones traverse the sea ice periphery and central Arctic, respectively. In addition, storms have larger spatial extent in 2016 with nonlocal implications.

Considering our second research question, namely storm impacts on sea ice in the context of the sea ice volume budget, we found that 2012 is characterized by thermodynamic storm impacts on sea ice volume in the Pacific sector, whereas 2016 is characterized more by combined thermodynamic and dynamical (convergence) storm impacts that counteract sea ice volume loss in the Pacific sector. Results from a local assessment of budget components further showed predominantly thermodynamic with some dynamic contributions near the sea ice edge and north of the CAA in 2012, and thermodynamic and dynamic contributions in the Pacific and central Arctic (north of the Laptev Sea) in 2016, as demonstrated by a thermodynamic/dynamic index Q_{td} documenting relative contributions.

In consideration of our third research question, differences between the 2012 and 2016 SIE are therefore attributed to differences in storm timing and location; whereas 2012 is distinguished by extreme cyclones near the sea ice edge in the Pacific sector and thin ice regime which quickly removed the sea ice cover in that region, 2016 is characterized by extreme cyclones over the central Arctic and thick ice regime.

The prominent role played by storm location and timing in sea ice loss is of particular interest when considering sea ice conditions in summer of 2019 and 2020. Although May and August 2019 experienced the second warmest air temperatures on record for the Arctic region, and the ice extent tracked below that of 2012 from the end of February through mid-June and then again from the beginning of July through to early August, the summertime minimum SIE was not comparable to that of 2012. Similarly, 2020 experienced both unusually warm temperatures and an extreme cyclone over the Beaufort Sea in July, which helped lead to the lowest July SIE on record, and second lowest summertime minimum SIE (NSIDC Arctic Sea Ice News and Analysis, August and September 2020; http://nsidc.org/arcticseaicenews/2020/08/ and http://nsidc.org/arcticseaicenews/2020/09/). The absence of a record minimum in SIE both in 2019 and 2020 despite record warm summers, combined with results from this analysis, suggest that the extreme storm of 2012 was key to reaching the record minimum that year. Other aspects of extremity, such as persistence of anomalously low sea level pressure (e.g., 2002) or persistence of anomalously high sea level pressure (e.g., 2007) patterns in summer can also lead to anomalously low September sea ice conditions (Serreze et al. 2003; Ogi et al. 2008; Stroeve et al. 2008; Hutchings and Rigor 2012). However, extreme storms like those in 2012 and 2016 have major impacts on comparably short time scales. Our results emphasize that extreme events are required to precipitate significant sea ice loss relative to the long-term mean, and furthermore that storm timing and location are instrumental in the nature of this loss.

Summer cyclones can have significant implications on regional scales for northern coastal communities and on hemispheric scales for international shipping, navigation, and cooperation,

particularly in the context of a changing climate. The question remains as to the relevance of this work for society and in the context of a changing climate. Can the results from this analysis be used in identifying extreme cyclone/storm-sensitive regions to prioritize protected areas and corridors? How well do models capture extreme cyclone impacts on sea ice? Characterization of relative thermodynamic and dynamic contributions to changes in Arctic sea ice volume during extreme cyclones offers a template for Q_{td} index probability maps illustrating and documenting local and regional thermodynamic and dynamic systems in the Arctic on a seasonal basis. As such, the present study can be used as a prelude to sea ice volume budget evaluations during summer using satellite-derived sea ice thickness estimates from *ICESat-2*. This will additionally enable observational–modeling comparisons and contribute to improved understanding of the physical mechanisms that characterize and describe extreme cyclone impacts on sea ice.

Acknowledgments. This work was funded by the Canada C-150 Chair program (Julienne Stroeve), NERC NE/R017123/1 (Julienne Stroeve), and the National Science Foundation (OPP-1748325) (Lawrence Hamilton) (NSFGEO-NERC Advancing Predictability of Sea Ice: Phase 2 of the Sea Ice Prediction Network (SIPN2)). MT acknowledges support from the Natural Environment Research Council Project "PRE-MELT" under Grant NE/T000546/1. FM is a F.R.S.-FNRS Research Fellow. HH is a UCL Postdoctoral Research Fellow. The authors thank Scott Stewart for providing the NSIDC sea ice drift data set without the buoy data incorporated.

REFERENCES

Akperov, M., I. Mokhov, A. Rinke, K. Dethloff, and H. Matthes, 2015: Cyclones and their possible changes in the Arctic by the end of the twenty first century from regional climate model simulations. *Theor. Appl. Climatol.*, **122**, 85–96, https://doi.org/10.1007/s00704-014-1272-2.

Bitz, C., M. M. Holland, E. C. Hunke, and R. E. Moritz, 2005: Maintenance of the sea-ice edge. *J. Climate*, **18**, 2903–2921, https://doi.org/10.1175/JCLI3428.1.

Cai, L., V. A. Alexeev, and J. E. Walsh, 2020: Arctic sea ice growth in response to synoptic- and large-scale atmospheric forcing from CMIP5 models. *J. Climate*, **33**, 6083–6099, https://doi.org/10.1175/JCLI-D-19-0326.1.

Cavalieri, D. J., C. L. Parkinson, P. Gloersen, and H. J. Zwally, 1997: Arctic and Antarctic sea ice concentrations from multichannel passive-microwave satellite data sets: October 1978–September 1995—User's guide. NASA Tech. Memo. 104647, 17 pp., https://ntrs.nasa.gov/api/citations/19980076134/downloads/19980076134.pdf.

Crawford, A. D., and M. C. Serreze, 2016: Does the summer Arctic frontal zone influence Arctic Ocean cyclone activity? *J. Climate*, **29**, 4977–4993, https://doi.org/10.1175/JCLI-D-15-0755.1.

——, and ——, 2017: Projected changes in the Arctic frontal zone and summer Arctic cyclone activity in the CESM large ensemble. *J. Climate*, **30**, 9847–9869, https://doi.org/10.1175/JCLI-D-17-0296.1.

Day, J. J., M. Holland, and K. I. Hodges, 2018: Seasonal differences in the response of Arctic cyclones to climate change in CESM1. *Climate Dyn.*, **50**, 3885–3903, https://doi.org/10.1007/s00382-017-3767-x.

Duarte, P., A. Sundfjord, A. Meyer, S. R. Hudson, G. Spreen, and L. H. Smedsrud, 2020: Warm Atlantic water explains observed sea ice melt rates north of Svalbard. *J. Geophys. Res. Oceans*, **125**, e2019JC015662, https://doi.org/10.1029/2019JC015662.

Fetterer, F., K. Knowles, W. N. Meier, M. Savoie, and A. K. Windnagel, 2017 (updated daily): Sea ice index, version 3. National Snow and Ice Data Center, accessed 26 April 2020, https://doi.org/10.7265/N5K072F8.

Finocchio, P. M., J. D. Doyle, D. P. Stern, and M. G. Fearon, 2020: Short-term impacts of Arctic summer cyclones on sea ice extent in the marginal ice zone. *Geophys. Res. Lett.*, **47**, e2020GL088338, https://doi.org/10.1029/2020GL088338.

Graham, R. M., and Coauthors, 2019: Winter storms accelerate the demise of sea ice in the Atlantic sector of the Arctic Ocean. *Sci. Rep.*, **9**, 9222, https://doi.org/10.1038/s41598-019-45574-5.

Guemas, V., F. Doblas-Reyes, A. Germe, M. Chevallier, and D. Salas y Mélia, 2013: September 2012 Arctic sea ice minimum: Discriminating between sea ice memory, the August 2012 extreme storm and prevailing warm conditions [in "Explaining Extreme Events of 2012 from a Climate Perspective"]. *Bull. Amer. Meteor. Soc.*, **94**, S20–S22, https://doi.org/10.1175/BAMS-D-13-00085.1.

Hamilton, L. C., and J. Stroeve, 2016: 400 predictions: The SEARCH sea ice outlook 2008–2015. *Polar Geogr.*, **39**, 274–287, https://doi.org/10.1080/1088937X.2016.1234518.

Heorton, H., and Coauthors, 2020: https://github.com/CPOMUCL/Budget_tool.

Holland, P. R., and R. Kwok, 2012: Wind-driven trends in Antarctic sea ice drift. *Nat. Geosci.*, **5**, 872–875, https://doi.org/10.1038/ngeo1627.

——, and N. Kimura, 2016: Observed concentration budgets of Arctic and Antarctic sea ice. *J. Climate*, **29**, 5241–5429, https://doi.org/10.1175/JCLI-D-16-0121.1.

Hutchings, J. K., and I. G. Rigor, 2012: Role of ice dynamics in anomalous ice conditions in the Beaufort Sea during 2006 and 2007. *J. Geophys. Res.*, **117**, C00E04, https://doi.org/10.1029/2011JC007182.

Jakobson, L., T. Vihma, and E. Jakobson, 2019: Relationships between sea ice concentration and wind speed over the Arctic Ocean during 1979–2015. *J. Climate*, **32**, 7783–7796, https://doi.org/10.1175/JCLI-D-19-0271.1.

Kay, J. E., T. L'Ecuyer, A. Gettelman, G. Stephens, and C. O'Dell, 2008: The contribution of cloud and radiation anomalies to the 2007 Arctic sea ice extent minimum. *Geophys. Res. Lett.*, **35**, L08503, https://doi.org/10.1029/2008GL033451.

Knudsen, E. M., Y. J. Orsolini, T. Furevik, and K. I. Hodges, 2015: Observed anomalous atmospheric patterns in summers of unusual Arctic sea ice melt. *J. Geophys. Res. Atmos.*, **120**, 2595–2611, https://doi.org/10.1002/2014JD022608.

Kriegsmann, A., and B. Brümmer, 2014: Cyclone impact on sea ice in the central Arctic Ocean: A statistical study. *Cryosphere*, **8**, 303–317, https://doi.org/10.5194/tc-8-303-2014.

Kwok, R., 2006: Contrasts in sea ice deformation and production in the Arctic seasonal and perennial ice zones. *J. Geophys. Res.*, **111**, C11S22, https://doi.org/10.1029/2005JC003246.

Lei, R., G. Dawei, P. Heil, J. K. Hutchings, and M. Ding, 2020: Comparisons of sea ice motion and deformation, and their responses to ice conditions and cyclonic activity in the western Arctic Ocean between two summers. *Cold Reg. Sci. Technol.*, **170**, 102925, https://doi.org/10.1016/j.coldregions.2019.102925.

Lynch, A. H., M. C. Serreze, E. N. Cassano, A. D. Crawford, and J. Stroeve, 2016: Linkages between Arctic summer circulation

regimes and regional sea ice anomalies. *J. Geophys. Res. Atmos.*, **121**, 7868–7880, https://doi.org/10.1002/2016JD025164.

Mayer, M., M. Alonso Balmaseda, and L. Haimberger, 2018: Unprecedented 2015/2016 Indo-Pacific heat transfer speeds up tropical Pacific heat recharge. *Geophys. Res. Lett.*, **45**, 3274–3284, https://doi.org/10.1002/2018GL077106.

Neu, U., and Coauthors, 2013: IMILAST: A community effort to intercompare extratropical cyclone detection and tracking algorithms. *Bull. Amer. Meteor. Soc.*, **94**, 529–547, https://doi.org/10.1175/BAMS-D-11-00154.1.

Notz, D., and J. Stroeve, 2018: The trajectory towards a seasonally ice-free Arctic Ocean. *Curr. Climate Change Rep.*, **4**, 407–416, https://doi.org/10.1007/s40641-018-0113-2.

——, and SIMIP Community, 2020: Arctic sea ice in CMIP6. *Geophys. Res. Lett.*, **47**, e2019GL086749, https://doi.org/10.1029/2019GL086749.

Ogi, M., I. G. Rigor, M. G. McPhee, and J. M. Wallace, 2008: Summer retreat of Arctic sea ice: Role of summer winds. *Geophys. Res. Lett.*, **35**, L24701, https://doi.org/10.1029/2008GL035672.

Olonscheck, D., T. Mauritsen, and D. Notz, 2019: Arctic sea-ice variability is primarily driven by atmospheric temperature fluctuations. *Nat. Geosci.*, **12**, 430–434, https://doi.org/10.1038/s41561-019-0363-1.

Parkinson, C. L., and J. C. Comiso, 2013: On the 2012 record low Arctic sea ice cover: combined impact of preconditioning and an August storm. *Geophys. Res. Lett.*, **40**, 1356–1361, https://doi.org/10.1002/grl.50349.

Perovich, D. K., and J. A. Richter-Menge, 2015: Regional variability in sea ice melt in a changing Arctic. *Philos. Trans. Roy. Soc.*, **373A**, 20140165, https://doi.org/10.1098/rsta.2014.0165.

——, T. C. Grenfell, J. A. Richter-Menge, B. Light, W. B. Tucker, and H. Eicken, 2003: Thin and thinner: Sea ice mass balance measurements during SHEBA. *J. Geophys. Res.*, **108**, 8050, https://doi.org/10.1029/2001JC001079.

Petty, A. A., J. C. Stroeve, P. R. Holland, L. N. Boisvert, A. C. Bliss, N. Kimura, and W. N. Meier, 2018: The Arctic sea ice cover of 2016: A year of record-low highs and higher-than-expected lows. *Cryosphere*, **12**, 433–452, https://doi.org/10.5194/tc-12-433-2018.

Pinto, J. G., T. Spangehl, U. Ulbrich, and P. Speth, 2005: Sensitivities of a cyclone detection and tracking algorithm: Individual tracks and climatology. *Meteor. Z.*, **14**, 823–838, https://doi.org/10.1127/0941-2948/2005/0068.

Rampal, P., J. Weiss, and D. Marsan, 2009: Positive trend in the mean speed and deformation rate of Arctic sea ice, 1979–2007. *J. Geophys. Res.*, **114**, C05013, https://doi.org/10.1029/2008JC005066.

Rinke, A., M. Maturilli, R. M. Graham, H. Matthes, D. Handorf, L. Cohen, R. Hudson, and J. C. Moore, 2017: Extreme cyclone events in the Arctic: Wintertime variability and trends. *Environ. Res. Lett.*, **12**, 094006, https://doi.org/10.1088/1748-9326/aa7def.

Rudeva, I., and I. Simmonds, 2015: Variability and trends of global atmospheric frontal activity and links with large-scale modes of variability. *J. Climate*, **28**, 3311–3330, https://doi.org/10.1175/JCLI-D-14-00458.1.

——, S. K. Gulev, I. Simmonds, and N. Tilinina, 2014: The sensitivity of characteristics of cyclone activity to identification procedures in tracking algorithms. *Tellus*, **66A**, 24961, https://doi.org/10.3402/tellusa.v66.24961.

Schreiber, E. A. P., and M. C. Serreze, 2020: Impacts of synoptic-scale cyclones on Arctic sea ice concentration: A systematic analysis. *Ann. Glaciol.*, **61**, 1–15, https://doi.org/10.1017/AOG.2020.23.

Schroeter, S., W. Hobbs, N. L. Bindoff, R. Massom, and R. Matear, 2018: Drivers of Antarctic sea ice volume change in CMIP5 models. *J. Geophys. Res. Oceans*, **123**, 7914–7938, https://doi.org/10.1029/2018JC014177.

Schweiger, A., R. Lindsay, J. Zhang, M. Steele, H. Stern, and R. Kwok, 2011: Uncertainty in modeled Arctic sea ice volume. *J. Geophys. Res.*, **116**, C00D06, https://doi.org/10.1029/2011JC007084.

Screen, J. A., I. Simmonds, and K. Keay, 2011: Dramatic interannual changes of perennial Arctic sea ice linked to abnormal summer storm activity. *J. Geophys. Res.*, **116**, D15105, https://doi.org/10.1029/2011JD015847.

Semenov, A., X. Zhang, A. Rinke, W. Dom, and K. Dethloff, 2019: Arctic intense summer storms and their impacts on sea ice—A regional climate modeling study. *Atmosphere*, **10**, 218, https://doi.org/10.3390/atmos10040218.

Serreze, M. C., 1995: Climatological aspects of cyclone development and decay in the Arctic. *Atmos.–Ocean*, **33** (1), 1–23, https://doi.org/10.1080/07055900.1995.9649522.

——, and A. P. Barrett, 2008: The summer cyclone maximum over the central Arctic Ocean. *J. Climate*, **21**, 1048–1065, https://doi.org/10.1175/2007JCLI1810.1.

——, and Coauthors, 2003: A record minimum Arctic sea ice extent and area in 2002. *Geophys. Res. Lett.*, **30**, 1110, https://doi.org/10.1029/2002GL016406.

Simmonds, I., and K. Keay, 2009: Extraordinary September Arctic sea ice reductions and their relationships with storm behaviour over 1979 to 2008. *Geophys. Res. Lett.*, **36**, L19715, https://doi.org/10.1029/2009GL039810.

——, and I. Rudeva, 2012: The great Arctic cyclone of August 2012. *Geophys. Res. Lett.*, **39**, L23709, https://doi.org/10.1029/2012GL054259.

——, and ——, 2014: A comparison of tracking methods for extreme cyclones in the Arctic basin. *Tellus*, **66A**, 25252, https://doi.org/10.3402/tellusa.v66.25252.

——, C. Burke, and K. Keay, 2008: Arctic climate change as manifest in cyclone behaviour. *J. Climate*, **21**, 5777–5796, https://doi.org/10.1175/2008JCLI2366.1.

Sorteberg, A., and J. E. Walsh, 2008: Seasonal cyclone variability at 70°N and its impact on moisture transport into the Arctic. *Tellus*, **60A**, 570–586, https://doi.org/10.1111/j.1600-0870.2008.00314.x.

Stroeve, J., and D. Notz, 2018: Changing state of Arctic sea ice across all seasons. *Environ. Res. Lett.*, **13**, 103001, https://doi.org/10.1088/1748-9326/aade56.

——, M. Serreze, S. Drobot, S. Gearheard, M. Holland, J. Maslanik, W. Meier, and T. Scambos, 2008: Arctic sea ice extent plummets in 2007. *Eos, Trans. Amer. Geophys. Union*, **89**, 13–14, https://doi.org/10.1029/2008EO020001.

——, L. C. Hamilton, C. M. Bitz, and E. Blanchard-Wrigglesworth, 2014: Predicting September sea ice: Ensemble skill of the SEARCH sea ice outlook 2008–2013. *Geophys. Res. Lett.*, **41**, 2411–2418, https://doi.org/10.1002/2014GL059388.

Tsamados, M., D. Feltham, A. Petty, D. Schroeder, and D. Flocco, 2015: Processes controlling surface, bottom and lateral melt of Arctic sea ice in a state of the art sea ice model. *Philos. Trans. Roy. Soc.*, **373A**, 20140167, https://doi.org/10.1098/rsta.2014.0167.

Tschudi, M., W. N. Meier, J. S. Stewart, C. Fowler, and J. Maslanik. 2019: Polar pathfinder daily 25 km EASE-grid sea ice motion vectors, version 4, daily. NASA National Snow and Ice Data Center Distributed Active Archive Center, accessed 7 September 2020, https://doi.org/10.5067/INAWUWO7QH7B.

Vessey, A. F., K. I. Hodges, L. C. Shaffrey, and J. J. Day, 2020: An inter-comparison of Arctic synoptic scale storms between four global reanalysis datasets. *Climate Dyn.*, **54**, 2777–2795, https://doi.org/10.1007/s00382-020-05142-4.

Wang, Z., J. Walsh, S. Szymborski, and M. Peng, 2020: Rapid Arctic sea ice loss on the synoptic time scale and related atmospheric circulation anomalies. *J. Climate*, **33**, 1597–1617, https://doi.org/10.1175/JCLI-D-19-0528.1.

Wernli, H., and L. Papritz, 2018: Role of polar anticyclones and mid-latitude cyclones for Arctic summertime sea-ice melting. *Nat. Geosci.*, **11**, 108–113, https://doi.org/10.1038/s41561-017-0041-0.

West, A., M. Collins, E. Blockley, J. Ridley, and A. Bodas-Salcedo, 2019: Induced surface fluxes: A new framework for attributing Arctic sea ice volume balance biases to specific model errors. *Cryosphere*, **13**, 2001–2022, https://doi.org/10.5194/tc-13-2001-2019.

Yamagami, A., M. Matsuda, and H. Tanaka, 2017: Extreme Arctic cyclone in August, 2016. *Atmos. Sci. Lett.*, **18**, 307–314, https://doi.org/10.1002/asl.757.

Zhang, J., R. Lindsay, A. Schweiger, and M. Steele, 2013: The impact of an intense summer cyclone on 2012 Arctic sea ice retreat. *Geophys. Res. Lett.*, **40**, 720–726, https://doi.org/10.1002/GRL.50190.